Yuan et al. *Zool. Res.* 2022, 43(5): 886−896
https://doi.org/10.24272/j.issn.2095-8137.2022.185

ZR | Zoological Research

Article Open Access

General mechanism of spider toxin family I acting on sodium channel Nav1.7

Fu-Chu Yuan[1,#], Fu-De Sun[2,#], Lin Zhang[1], Biao Huang[3], Hai-Long An[2], Ming-Qiang Rong[1,*], Can-Wei Du[3,*]

[1] *National & Local Joint Engineering Laboratory of Animal Peptide Drug Development*, *College of Life Sciences*, *Hunan Normal University*, *Changsha*, *Hunan* 410006, *China*

[2] *Key Laboratory of Molecular Biophysics*, *Hebei Province*, *Institute of Biophysics*, *School of Health Science & Biomedical Engineering*, *Hebei University of Technology*, *Tianjin* 300401, *China*

[3] *Chengdu Pepbiomedical Co., Ltd.*, *Chengdu*, *Sichuan* 610219, *China*

ABSTRACT

Various peptide toxins in animal venom inhibit voltage-gated sodium ion channel Nav1.7, including Nav-targeting spider toxin (NaSpTx) Family I. Toxins in NaSpTx Family I share a similar structure, i.e., N-terminal, loops 1–4, and C-terminal. Here, we used Mu-theraphotoxin-Ca2a (Ca2a), a peptide isolated from *Cyriopagopus albostriatus*, as a template to investigate the general properties of toxins in NaSpTx Family I. The toxins interacted with the cell membrane prior to binding to Nav1.7 via similar hydrophobic residues. Residues in loop 1, loop 4, and the C-terminal primarily interacted with the S3–S4 linker of domain II, especially basic amino acids binding to E818. We also identified the critical role of loop 2 in Ca2a regarding its affinity to Nav1.7. Our results provide further evidence that NaSpTx Family I toxins share similar structures and mechanisms of binding to Nav1.7.

Keywords: Spider; Nav1.7; Peptide toxin; ICK motif

INTRODUCTION

Voltage-gated sodium channels (VGSCs or Navs) are essential for the initiation and propagation of action potentials in excitable tissues, such as nerves and muscles, and in excitable cells (Cummins et al., 2004; Dib-Hajj et al., 2013; Faber et al., 2012; Weiss et al., 2011). Nine Navs (Nav1.1–Nav1.9) have been identified in humans. Nav1.7 is located in the peripheral nervous system and consists of a pore-forming α subunit and β1/β2 subunits (Shen et al., 2019). The α subunit acts as a heterotetramer (DI–DIV), and each domain contains six α-helical transmembrane segments (S1–S6). Segments S1–S4 form a voltage-sensing domain and segments S5–S6 form a pore-forming region as the Na^+ selectivity filter near the extracellular side (Payandeh et al., 2011, 2012; Yu & Catterall, 2003). Nav channels are targeted by various natural toxins and at least seven binding sites have been identified (McCormack et al., 2013). Small molecule neurotoxins, such as tetrodotoxin (TTX) and saxitoxin (STX), function as pore blockers on Nav channels (Ahuja et al., 2015), while most peptide toxins interact with the S3–S4 linker of Nav channels as gating modifier toxins (Xu et al., 2019). As gain-of-function mutation in Nav1.7 can induce severe irregular pain in genetic neuropathies (Dib-Hajj et al., 2013)

Received: 08 July 2022; Accepted: 01 September 2022; Online: 02 September 2022

Foundation items: This work was supported by the National Natural Science Foundation of China (31971190), Science Fund for Distinguished Young Scholars of Hunan Province (2021JJ10035), Education Department of Hunan Province (19A321)

[#]Authors contributed equally to this work

*Corresponding authors, E-mail: rongmq@hunnu.edu.cn; ducw2022@163.com

and loss-of-function mutation can cause congenital insensitivity to pain (Cox et al., 2006), selective inhibitors of Nav1.7 are presumed to be potent analgesics for pain treatment (Minett et al., 2012; Yang et al., 2013). Thus, toxins showing specific activity against Nav1.7 may offer potential therapeutics for pain management (Klint et al., 2012).

Spider venom is comprised of many proteins and peptides. To date, more than 60 peptides acting on sodium channels have been reported in the UniProt database, which are classified into 12 families (Nav-targeting spider toxin, NaSpTx I–XII) based on their conserved sequences and intra-cystine spacing (Klint et al., 2012). NaSpTx Family I has been studied for many years and several well-known toxins, such as Beta-theraphotoxin-Cm1a (CcoTX-I) from *Ceratogyrus marshalli* (Shcherbatko et al., 2016), Huwentoxin-IV (HWTX-IV) from *Cyriopagopus schmidti* (Agwa et al., 2017), and Mu-theraphotoxin-Hhn1b 1 (HNTX-IV) from *Cyriopagopus hainanus* (Li et al., 2004), show excellent effects on human Nav1.7. These toxins typically consist of 33–35 residues and three disulfide bonds (C1–C4, C2–C5, and C3–C6), which are important for the inhibitor cystine knot (ICK) motif. The NaSpTx Family I toxins fold into spheres in native conformation and their primary structure is divided into six parts, i.e., N-terminal, loops 1–4, and C-terminal (Klint et al., 2015).

Toxins in NaSpTx Family I primarily bind to the S3–S4 linker in the second voltage sensor domain (VSDII) of human Nav1.7, termed “site 4” (Wisedchaisri et al., 2021). Toxins bind to anionic lipids through hydrophobic and electrostatic interactions, after which key residues of toxins interact with corresponding residues in Nav1.7 (Agwa et al., 2017). The mutants of some toxins, such as CcoTX-I (Shcherbatko et al., 2016), HWTX-IV (Agwa et al., 2017), and HNTX-III (Li et al., 2004), have demonstrated that motif -WCKY- at the C-terminal, phenylalanine at loop 1, and residues at position 28/29 in loop 3 affect the inhibitory activity of toxins on Nav1.7. Furthermore, mutations of E818, L823, V824, and F826 in domain II of Nav1.7 significantly reduce the affinity of toxins to the channel (Wisedchaisri et al., 2021; Xiao et al., 2008; Zhang et al., 2021).

Mu-theraphotoxin-Ca2a (Ca2a), a 35-residue peptide isolated from the *Cyriopagopus albostriatus* spider and belonging to NaSpTx Family I, is proposed to alleviate pain behaviors in mice by targeting Nav1.7 (Zhang et al., 2018). In this study, we compared the structures and functions of several toxins in NaSpTx Family I, including Ca2a, to reveal the general characteristics of NaSpTx Family I toxins that inhibit Nav1.7. Our results should help elucidate the mechanism by which NaSpTx Family I toxins act on Nav1.7 and provide clues for the design of selective peptide drugs targeting Nav1.7.

MATERIALS AND METHODS

Sequence alignment and homologous modeling

Sequences of Ca2a and other toxins in NaSpTx Family I were obtained from the UniProt database, and alignment was performed using MEGA v11. The Swiss-model website (https://swissmodel.expasy.org) was used to build the structure of Ca2a. After downloading the Ca2a model, it was checked using Ramachandran Plot (http://services.mbi.ucla.edu/SAVES/) and optimized using Discovery Studio 2019.

Molecular docking

ZDOCK was used to dock the NaSpTx Family I toxins with activated human Nav1.7 (PDB ID: 6n4q). Parameters were set as follows: angular step size, 6°; root mean square deviation (RMSD) cutoff, 6.0 Å; interface cutoff, 9.0; maximum number of clusters, 60; and receptor binding site residues, E818. RDOCK was used to refine the ZDOCK results, and higher docking poses were ranked using the ZDOCK score. The lowest energy value pose was chosen according to E_RDOCK of RDOCK.

Cell culture and transfection

HEK293T cells were cultured in Dulbecco’s Modified Eagle Medium (DMEM) containing 10% fetal bovine serum in 5% CO_2 under 37 °C. The medium was replaced by Opti-MEM before transfection. Wild-type (WT) and E818A plasmids of the human Nav1.7 (hNav1.7) channel were incubated with Lipofectamine 2000 for 30 min in Opti-MEM and enhanced green fluorescent protein (eGFP) was transfected into cells at the same time. After 4–6 h, cells were plated in fresh DMEM. Cells showing green fluorescence were used to check hNav1.7 channel currents after 15 h of transfection.

Peptide purification, refolding, and mass spectrometry identification

The Ca2a peptide and its mutants were synthesized following our previous report (Zhang et al., 2018). The synthesized linear peptide was purified using semi-industrial reverse-phase high-performance liquid chromatography (HPLC) (C18 column, 10 mm×250 mm), with acetonitrile concentration varying at 1%/min. Ca2a was collected and lyophilized. The lyophilized linear peptide was then dissolved in deoxygenated refolding buffer containing 0.1 mol/L NaCl, 0.1 mol/L Tris-HCl, 5 mmol/L glutathione (GSH), and 0.5 mmol/L oxidized glutathione (GSSG) , pH 7.5–7.9. After 24 h at 4 °C, 1% trifluoroacetic acid (TFA) was used to stop the reaction. The oxidized peptide was purified via semi-preparative reversed-phase HPLC (C18 column, 10 mm×250 mm). Matrix-assisted laser desorption/ionization-time-of-flight mass spectrometry (MALDI-TOF MS) was performed to identify molecular weight.

Electrophysiology

Currents of hNav1.7 and its mutants in HEK293T cells were obtained using an EPC 10 USB Patch Clamp Amplifier (HEKA, Elektronik) at room temperature. For whole-cell patch-clamp recordings, the intracellular solution contained (mmol/L) 140 CsCl, 10 NaCl, 1 EGTA, and 10 HEPES (pH 7.4, adjusted with CsOH) and the extracellular solution contained (mmol/L) 140 NaCl, 2 $CaCl_2$, 1 $MgCl_2$, 5 KCl, 20 HEPES, and 10 glucose (pH 7.4, adjusted with NaOH). The pipette was polished with an access resistance of 2.0–3.0 MΩ. The HEK293T cells were held at −80 mV for all parameters examined. Macroscopic sodium currents were filtered at 5 kHz and sampled at 20 kHz. To reduce voltage errors, series resistance compensation was applied at 75%. The hNav1.7

channel currents were elicited by 50 ms depolarization potential to 0 mV from −80 mV. All chemicals were purchased from Sigma. Data were acquired using Patch Master (HEKA, Elektronik).

Mutation energy calculation

The peptide-hNav1.7 complex was first processed, and CHARMM was used as the force field. Replace New Only was selected as the mode for residues within 3Å. Residues replaced by alanine were chosen. Signal mutation was then carried out, and other parameters were not altered. For saturation mutation scanning, key residues mutated to all other amino acids were chosen. Parameters was set the same as for virtual alanine scanning.

Simulation of peptide-membrane interaction

Simulations of protein-membrane interactions were constructed in GROMACS v5.1.2, with the Martini 2.0 coarse-grained (CG) force field used due to its long time-scale of huge membrane-peptide complexes (Marrink et al., 2007; Sun et al., 2020). The peptide structures were derived from the RCSB protein database and transferred to the CG models using the *martinize.py* tool, and secondary structures were defined by coiled coils. The lipid bilayer model with POPC:POPS (4:1) was used to mimic the bacterial membrane with *insane.py*. The peptide was placed above the membrane surface at a distance of 2.0 nm. The systems were then solvated and energy-minimized. Pre-equilibrium procedures were subsequently conducted using peptide backbone restraints and force constants of 1 000 kJ/(mol·nm^2) to prevent the peptides from moving. A shift cut-off method was applied for non-bonded interactions, and the Coulomb and Van der Waals interactions decreased to zero at 1.2 nm from 0.0 nm and 0.9 nm, respectively. After equilibration, the simulations were run with periodic boundary conditions and a time step of 20 fs. Simulation duration was set to 2.0 μs. Further details can be found in our previous work (Sun et al., 2017).

Data analysis

Data were analyzed using PatchMaster v2x73 (HEKA Elektronik), IgorPro8 (WaveMetrics, USA), GraphPad Prism v9 (GraphPad Software), and Office Excel 2019 (Microsoft, USA). Statistical analyses were performed with GraphPad Prism v9. All values are shown as mean±standard error of the mean (*SEM*) and represent the number of cells examined. The level of statistical significance was set to $P<0.05$.

RESULTS

NaSpTx Family I toxins showed similar structures

To further understand the relationship of Ca2a with other toxins in NaSpTx Family I and to reveal the general characteristics of NaSpTx Family I toxins, residue sequences of NaSpTx Family I toxins were obtained from UniProt. Alignment of Ca2a with NaSpTx Family I members showed that their sequences exhibited high homology (Figure 1A). Notably, Ca2a shared 82.9% identity with Mu-theraphotoxin-Hd1a from *Cyriopagopus doriae*, 68.6% identity with Beta-theraphotoxin-Ps1a from *Paraphysa scrofa*, and 62.9% identity with Mu-theraphotoxin-Hs2a from *Cyriopagopus schmidti*. Ca2a also contained six conserved cysteine residues critical for the formation of the ICK motif and a "-WCKY" motif near the C-terminal that is conserved in NaSpTx Family I (Figure 1A). In addition, several residues essential for the binding of toxins to the Nav channel (Minassian et al., 2013; Zhang et al., 2021) were conserved in NaSpTx Family I (Figure 1B), suggesting that NaSpTx Family I toxins may share a similar mechanism when acting on the channel.

As the crystalline structure of Ca2a has not yet been resolved, we performed homology modeling using Hd1a (PDB ID: 2mpq) as a template. The reliable modeling structure (valued at 0.74) indicated that Ca2a consisted of six parts, i.e., N-terminal, loops 1–4, and C-terminal (Figure 2A), and showed considerable overlap with Hd1a (Figure 2B). Similar structures were observed for the other five NaSpTx Family I toxins (Figure 2C, D) (HNTX-I, HWTX-IV, HNTX-IV, HNTX-III, and CcoTX-I), which showed similar inhibitory efficacy against Nav1.7. The pharmacophores of the five toxins targeting Nav1.7 and key functional residues on the three-dimensional (3D) structure of the toxins have been identified in previous work (Cardoso & Lewis, 2019; Carstens et al., 2011; de Lera Ruiz & Kraus, 2015). As the toxins exhibit similar mechanisms for targeting Nav1.7, we compared the structures of the toxins and key residues. The toxins exhibited a high degree of overlap in 3D structure due to the ICK skeleton (Figure 2A) and sequence similarity (Figure 1A). The structure of all NaSpTx Family I toxins consisted of an N-terminal, four loops, and a C-terminal. Loop 1 (3–8), loop 2 (10–15), and loop 4 (25–30) showed high overlap conformation among toxins, whereas loop 3 (18–23) showed a different conformation, leading to differences in structural conformation (Figure 2D). Therefore, those NaSpTx Family I toxins acting on Nav1.7, including the recently identified Ca2a, share similar structures.

NaSpTx Family I toxins inhibit Nav1.7 in a similar manner

To explore the interactions of the NaSpTx Family I toxins with Nav1.7, we carried out molecular docking. As shown in Figure 3A, B, four NaSpTx Family I toxins (HNTX-III (PDB ID: 2jtb, orange), HWTX-IV (PDB ID: 5t3m, blue), HNTX-IV (PDB ID: 1niy, cyan), and CcoTX-I (PDB ID: 6br0, yellow)) interacted with the activated state of Nav1.7 (PDB ID: 6n4q). Specifically, residue F5 in HNTX-III and residue K7 in HNTX-IV interacted with D816 in Nav1.7, and residue W28 in CcoTX-I, residue N19 in HNTX-III, residue K27 in HWTX-IV, and residue N10 in HNTX-IV interacted with E818 (Figure 3C). These results are consistent with previous studies (Bosmans et al., 2006; Wisedchaisri et al., 2021; Xiao et al., 2008), indicating that NaSpTx Family I toxins inhibit Nav1.7 via a similar mechanism.

We previously found that the domain II S3–S4 linker is essential for the binding of Ca2a to Nav1.7 and residue E818 plays a critical role in the inhibitory effects of Ca2a on the channel (Zhang et al., 2018). Here, to explore the interactions between Ca2a and Nav1.7, we performed molecular docking. Similar to HWTX-IV binding to Nav1.7 (Figure 3D), Ca2a anchored to the domain II S3–S4 linker and residue K32 bonded to residues D816 and E818 (Figure 3E, F). To identify critical residues of Ca2a acting on Nav1.7, we performed virtual alanine mutation scanning of the Ca2a and channel

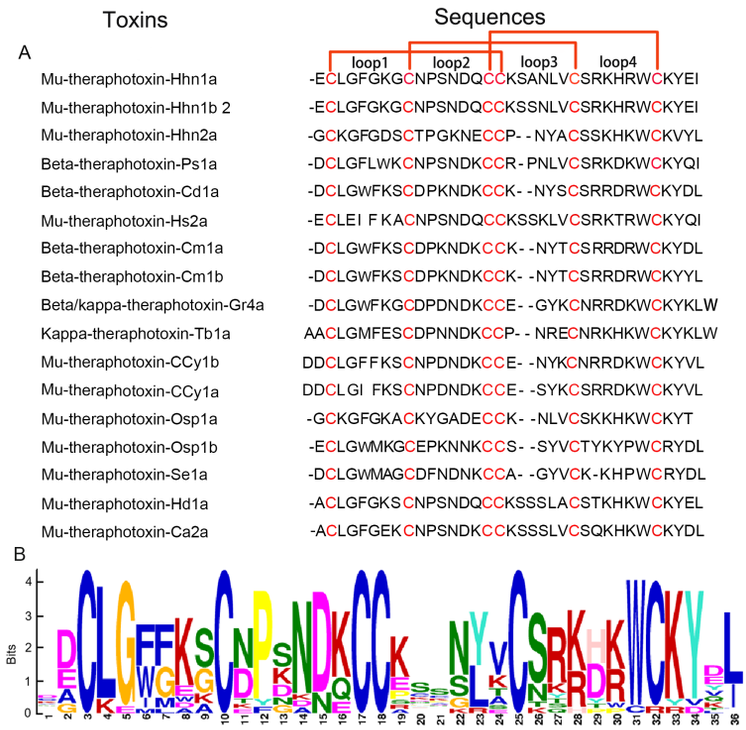

Figure 1 Sequence alignment of toxins in NaSpTx Family I

A: Results of multiple sequence alignment. Toxins were divided into N-terminal, four loops, and C-terminal. Intramolecular disulfide bonds C1–C4, C2–C5, and C3–C6 are labeled in red. B: Logo possibility of sequence MOTIF model. Letter size represents conservative level.

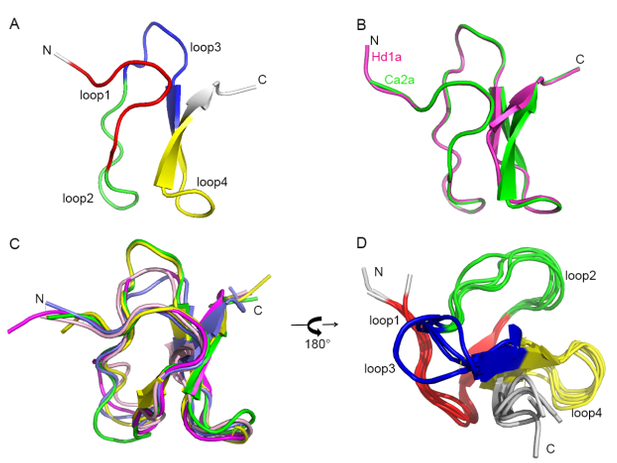

Figure 2 Spatial structure comparison of toxins in NaSpTx Family I

A: Homology modeling of Ca2a based on Hd1a. N-terminal, loops 1–4, and C-terminal are labeled. B: Comparison of structures of Hd1a (PDB ID: 2mpq) (magenta) and Ca2a (green). C: Overlap of five toxins in NaSpTx Family I, HNTX-I (magenta; PDB ID: 2mqf), HWTX-IV (green; PDB ID: 1mb6), HNTX-IV (cyan; PDB ID: 1niy), HNTX-III (pink; PDB ID: 2jtb), and CcoTX-I (slate; PDB ID: 6br0). D: View of spatial structure of five toxins from another side. Six structural divisions are labeled.

complex. As shown in Figure 4A, several residue mutations (F5A, K18A, W30A, K32A, Y33A, and D34A) reduced the affinity of Ca2a for Nav1.7. Patch-clamp recordings were performed to determine the effects of these mutants on Nav1.7. The K27A mutation significantly decreased (by 8.4-fold) the affinity of Ca2a for Nav1.7, with a half maximal inhibitory concentration (IC_{50}) of 4.07 μmol/L (Figure 4E). The W30A mutation markedly reduced the inhibitory effects of Ca2a on the channel, with a 20-fold increase in the IC_{50} compared to that of the WT peptide (Figure 4D, E). The K32A mutation resulted in a considerable loss of Ca2a sensitivity to Nav1.7, with an IC_{50} beyond the highest tested concentration (30 μmol/L) (Figure 4C, E). These results suggest that residues in loop 4 are essential for the function of Ca2a on Nav1.7.

To further analyze the interactions of Ca2a with Nav1.7, double-mutant cycle analysis was performed. Results showed that mutant K32A of Ca2a exhibited similar inhibitory activity against WT and mutant E818A of Nav1.7, and inhibition showed no significant difference from the effect of Ca2a on mutant E818A (Figure 5A, B), suggesting that residue K32 in Ca2a may interact directly with E818 of Nav1.7. In contrast, mutant K27A of Ca2a completely abolished the inhibitory activity on mutant E818A of Nav1.7 (Figure 5B), suggesting overlapping effects of residues K27 of Ca2a and E818 of Nav1.7 for the binding of Ca2a on Nav1.7. Virtual saturation mutation scanning showed that mutations in residues L3, F5, H28, W30, and Y33 may increase the affinity of Ca2a to Nav1.7 (Figure 5D). However, inhibitory efficacy showed that the F5K, H28K, W30K, and Y33K mutations in Ca2a exhibited significant loss-of-function against Nav1.7 (IC_{50}>20 μmol/L), with the H28R mutant showing a >30-fold in IC_{50} (14.87 μmol/L) compared with the WT peptide (Figure 5C).

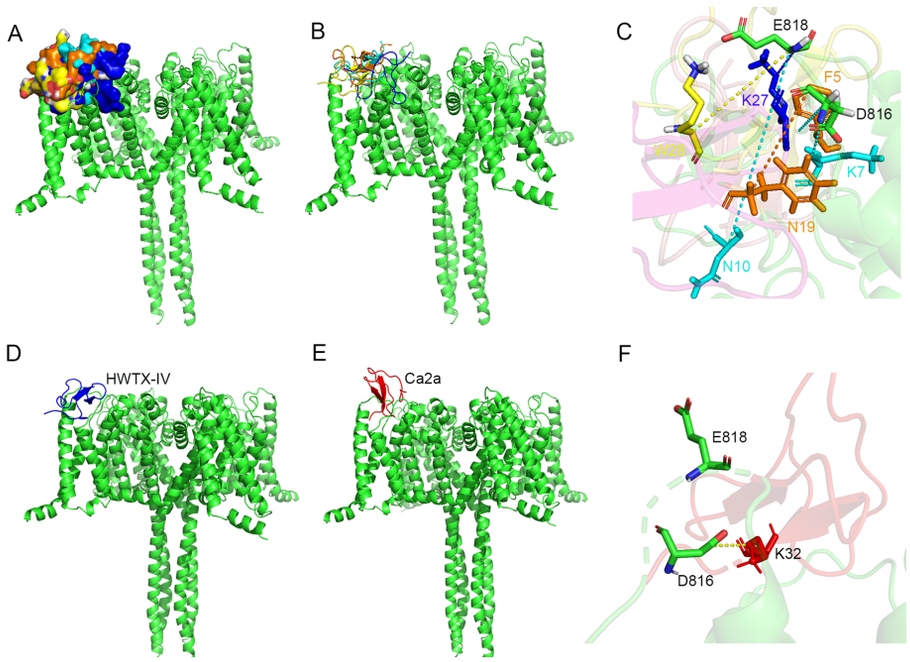

Figure 3 Molecular docking of toxins in NaSpTx Family I on hNav1.7 (PDB ID: 6n4q) domain II

A, B: Surface format (A) and cartoon format (B) of four toxins in NaSpTx Family I on hNav1.7, HNTX-III (orange), HWTX-IV (blue), HNTX-IV (cyan), and CcoTX-I (yellow). C: Critical residues for interactions of four toxins in NaSpTx Family I with hNav1.7 channel, F5 and N19 in HNTX-III (orange), K27 in HWTX-IV (blue), K7 and N10 in HNTX-IV (cyan), W28 in CcoTX-I (yellow), and D816 and E818 in hNav1.7 (green) are labeled. D: Molecular docking of HWTX-IV on hNav1.7. E, F: Molecular docking (E) and critical residues (F) of Ca2a on hNav1.7, K32 in Ca2a and D816 and E818 in hNav1.7 are labeled.

The above results suggest that the NaSpTx Family I toxins act on Nav1.7 in a similar manner as residues in loops 1 and 4 of the NaSpTx Family I toxins interact with the S3–S4 linker of domain II, especially the interaction of residue K32 of Ca2a with E818 of Nav1.7.

NaSpTx Family I toxins interact with cell membranes through hydrophobic residues

Certain NaSpTx Family I toxins can insert into the cell membrane before binding to Nav1.7 (Lawrence et al., 2019). Here, we used a protein-membrane control system to elucidate the interactions of NaSpTx Family I toxins (Ca2a and HWTX-IV) with the cell membrane. Beta/omega-theraphotoxin-Tp2a (ProTX-II) from *Thrixopelma pruriens* (Schmalhofer et al., 2008) (PDB ID: 5o0u), with a different inhibitory mechanism for Nav1.7, was used to analyze peptide-toxin interactions with the cell membrane (Xiao et al., 2010). POPC:POPS (4:1) was selected as the membrane, and Martini 2.0 coarse-grained force field conditions were applied as the simulated force field (2.0 μs simulation). As the peptide-membrane distance changed under varying simulation time, Ca2a and HWTX-IV adhered to the membrane surface rapidly, similar to ProTX-II (Figure 6A). However, Ca2a exhibited a higher probability of bilayer contact with the membrane (contact: 150) than HWTX-IV and ProTX-II (Figure 6B), suggesting that Ca2a may interact strongly with the hydrophobic region of the membrane. Several Ca2a residues (L3, F5, W30, and Y33) were inserted into the membrane (Figure 7A), similar to essential residues (I5, F6, W30, and Y33) in HWTX-IV (Figure 7C), suggesting that NaSpTx Family I toxins interact with the membrane in a similar manner as hydrophobic residues in the N- and C-terminals of toxins anchored to the membrane, which enhanced interactions with the Nav channel. The tryptophan residues (W5, W7, W24, and W30) in ProTX-II played important roles in toxin insertion into the membrane (Figure 7E). Based on quantitative analysis, these critical residues in the three peptides displayed higher contact with the cell membrane (Figure 7B, D, F), suggesting that Ca2a and HWTX-IV interact with the cell membrane via similar residues. Moreover, the membrane insertion depth of the three toxins did not differ significantly. Under coarse-grained simulation conditions, Ca2a and HWTX-IV did not show significant differences in adsorption capacity or action intensity of the membrane, which may be related to the equal charge of the two peptides. Although the specific amino acids involved differed significantly, toxins in NaSpTx Family I, Ca2a, and HWTX-IV showed similar insertion depth into the membrane.

Ca2a loop 2 is critical for Nav1.7 inhibition

Alignment of the NaSpTx Family I toxins revealed significant molecular diversity in the loop 2 sequences (Figure 1). Here, we explored the role of loop 2 residues in Ca2a interacting with Nav1.7, which may be conducive to obtaining shorter peptides. We first designed truncated peptide T1 using Ca2a as a template. As shown in Figure 8A, T1 displayed a moderately decreased affinity (IC_{50}=14.71 μmol/L) to Nav1.7 compared to WT Ca2a (Table 1), suggesting that loop 2 may be critical for the binding of Ca2a to Nav1.7. We next constructed two truncated peptides, T2 and T3, by deleting the

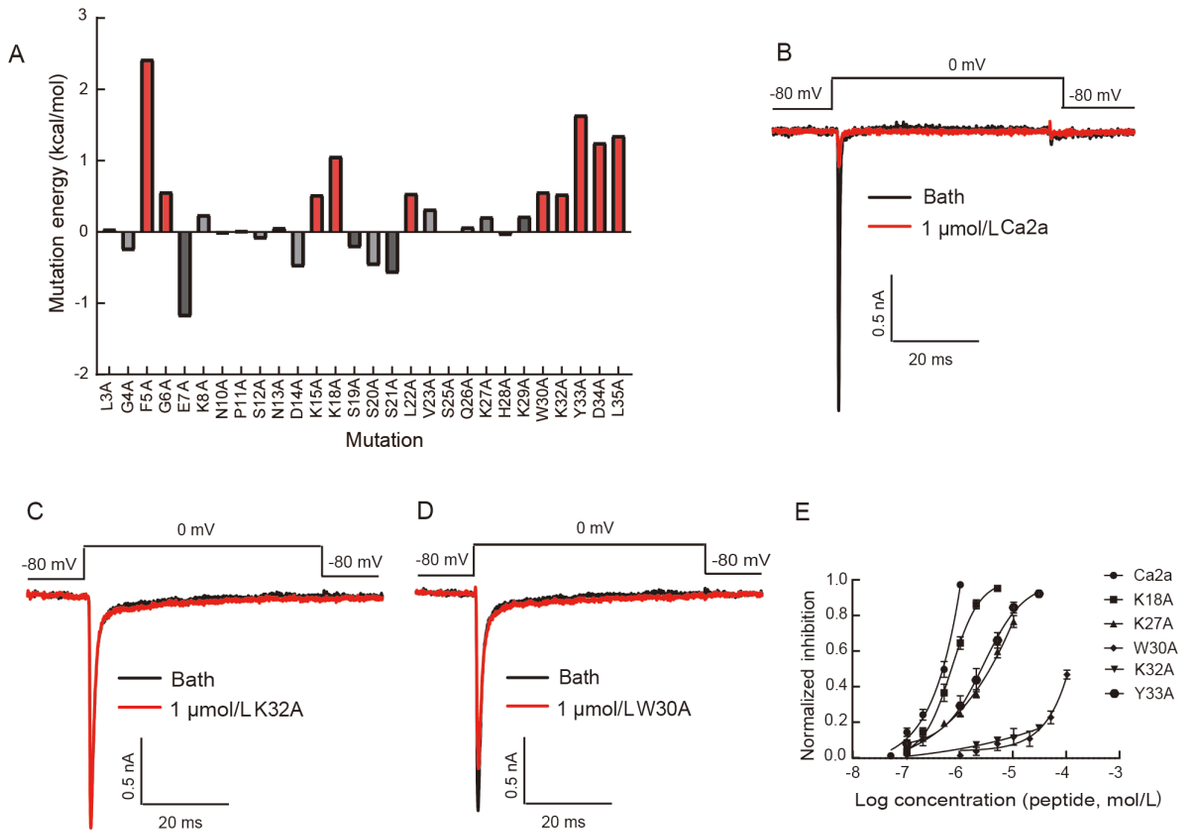

Figure 4 Effect of Ca2a and its alanine mutants on hNav1.7

A: Virtual alanine scanning of Ca2a to determine binding energy on hNav1.7. B–D: Inhibition of Ca2a (B), mutant K32A (C), and mutant W30A (D) on hNav1.7. Current was evoked by 0 mV potential and peptide (red line) was perfused on cells after currents were stable. E: Concentration-response curve of Ca2a and its mutants on Nav1.7. Data (n=4–6 for each data point) were fit by a Hill equation.

serine residue in loop 3 of Ca2a. This resulted in a reduction in the activity of Ca2a towards Nav1.7 (Figure 8A, B), thus suggesting the importance of the serine residue for the binding of Ca2a to Nav1.7. Next, residues L22 and V23 in loop 3 of Ca2a were deleted, resulting in the T4–T7 truncated peptides losing their affinity to Nav1.7 (IC_{50}>100 μmol/L) (Figure 8B; Table 1). Mutant K18A retained most of its inhibitory activity against Nav1.7 compared to Ca2a (Figure 4E). Surprisingly, deletion of K18 (mutant T8) dramatically decreased the activity of Ca2a against the channel (Figure 8B). We synthetized several additional truncated peptides (T9–T12) by deleting a single residue in loop 2. Results showed a medium reduction in affinity for Nav1.7 (Figure 8C), supporting the importance of loop 2 for the binding of Ca2a to the channel. Lastly, truncated peptide T13 showed higher inhibitory activity against Nav1.7 compared to the other truncated peptides, although more residues were deleted (Figure 8A). Circular dichroism (CD) spectra showed that the basic skeletons of the 13 peptides were not altered and were similar to that of the WT peptide (Figure 8D–F). However, the absorbance values of the modified peptides were higher than that of other peptides due to possible changes in the number and characteristics of residues or the size and morphology of secondary structures. Therefore, loop 2 may be important for the ICK skeleton and NaSpTx Family I toxin functions against the channel.

DISCUSSION

Animal venom is an important bioresource for drug discovery and critical for animal survival and predation (Zhang, 2015). Animal toxins exhibit various biological functions, including interactions with certain enzymes and regulation of ion channels (Kalia et al., 2015). Toxins are evolutionarily diverse but common in many poisonous and venomous animals (Hayes & Van Melderen, 2011), e.g., SsTX toxin family in centipedes (Du et al., 2019; Luo et al., 2018; Tang et al., 2021) and SHK toxin family in sea anemones (Kalman et al., 1998). In this study, we compared the structures and functions of NaSpTx Family I toxins acting on the Nav1.7 channel. Sequence alignment (Figure 1) and homology modeling (Figure 2) showed that the NaSpTx Family I toxins exhibited similar structures, including the same cysteine position and similar four-loop conformation. Based on molecular docking, we found that NaSpTx Family I toxins (including HNTX-III, HWTX-IV, and Ca2a) were anchored at the domain II S3–S4 linker of Nav1.7 and similar residues were involved in the binding of the toxins to Nav1.7 (Figure 3), consistent with previous studies (Liu et al., 2013; Xiao et al., 2008). Notably, residue F5 in HNTX-III, residue W28 in CcoTX-I, and residue N19 in HNTX-III interacted with Nav1.7 via π bonds, while residues K7 and K27 in HWTX- IV interacted with Nav1.7 via ionic bonds with acidic residues. Peptide-membrane

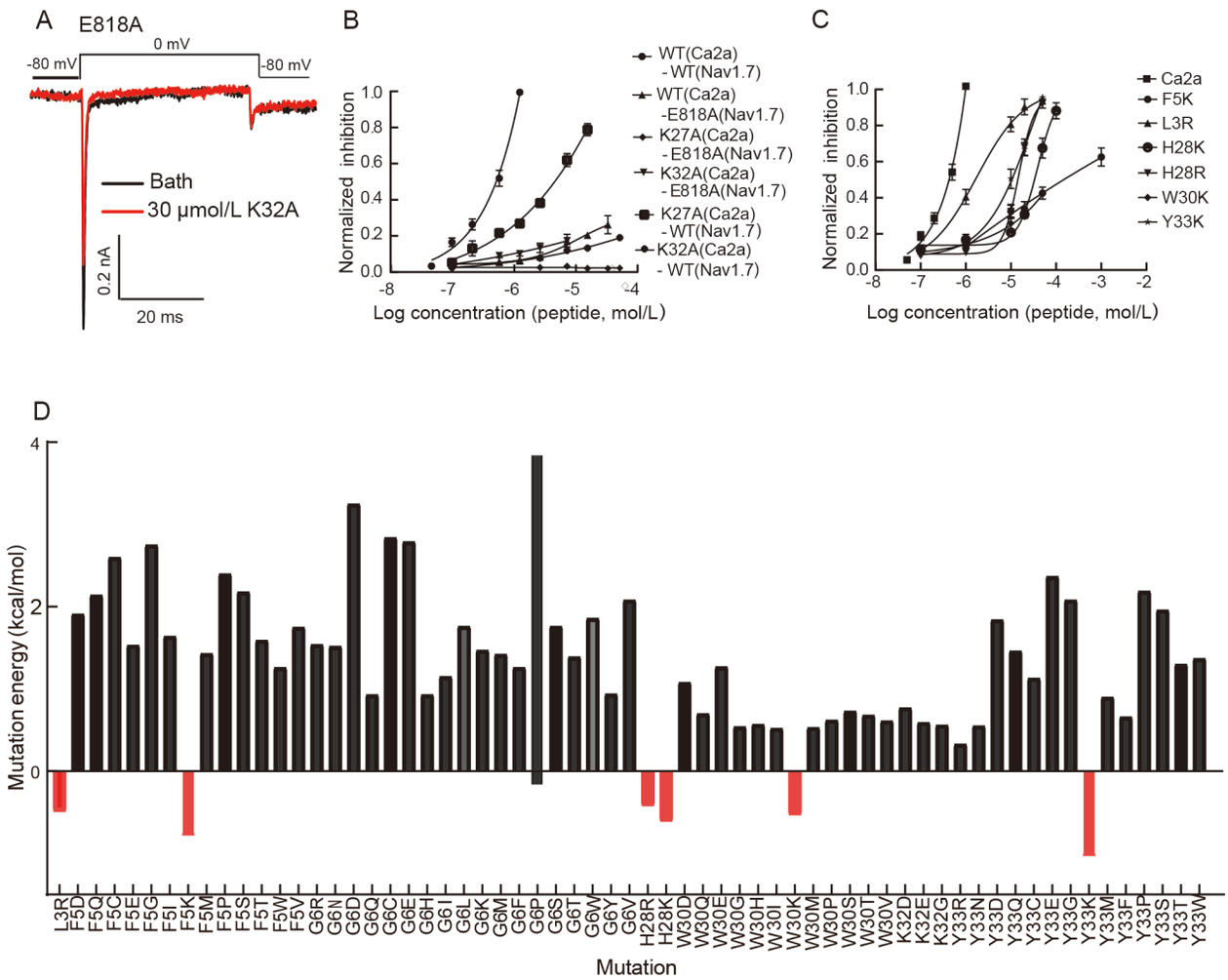

Figure 5 Effect of Ca2a mutants on hNav1.7 channel

A: Inhibition of Ca2a mutant K32A on E818A in hNav1.7 channel. B: Double-mutant cycle analysis of interactions of K32 and K27 in Ca2a with E818A in Nav1.7. C: Concentration-response curve of Ca2a and its mutants on Nav1.7 based on hNav1.7 and mutants obtained from saturation mutations in Figure 5D. Data are mean±*SEM*, *n*=4–6 cells per data point. D: Saturation mutation energy of residues in Ca2a binding to hNav1.7.

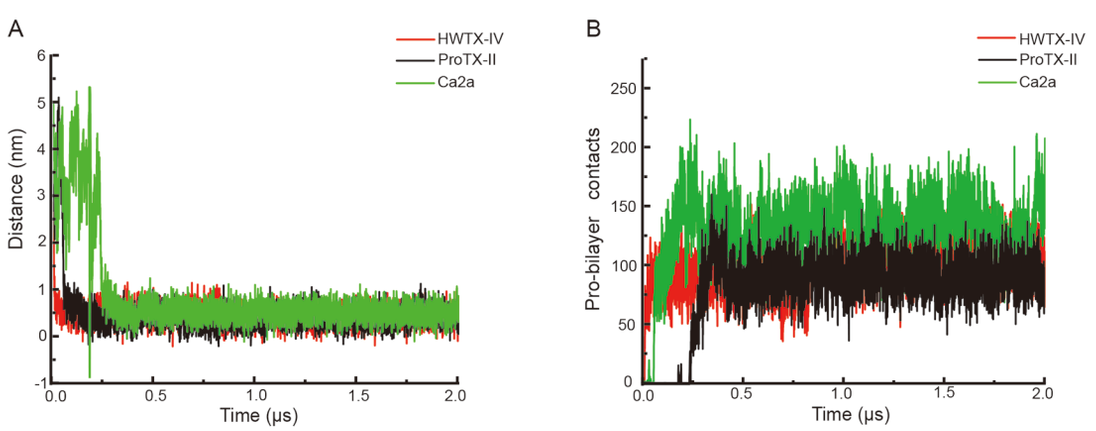

Figure 6 Action of three toxins with cell membrane

A: Distance change of three toxins attaching to cell membrane, Ca2a (green), HWTX-IV (red), and ProTX-II (black). B: Action intensity of three toxins on cell membrane, Ca2a (green), HWTX-IV (red), and ProTX-II (black).

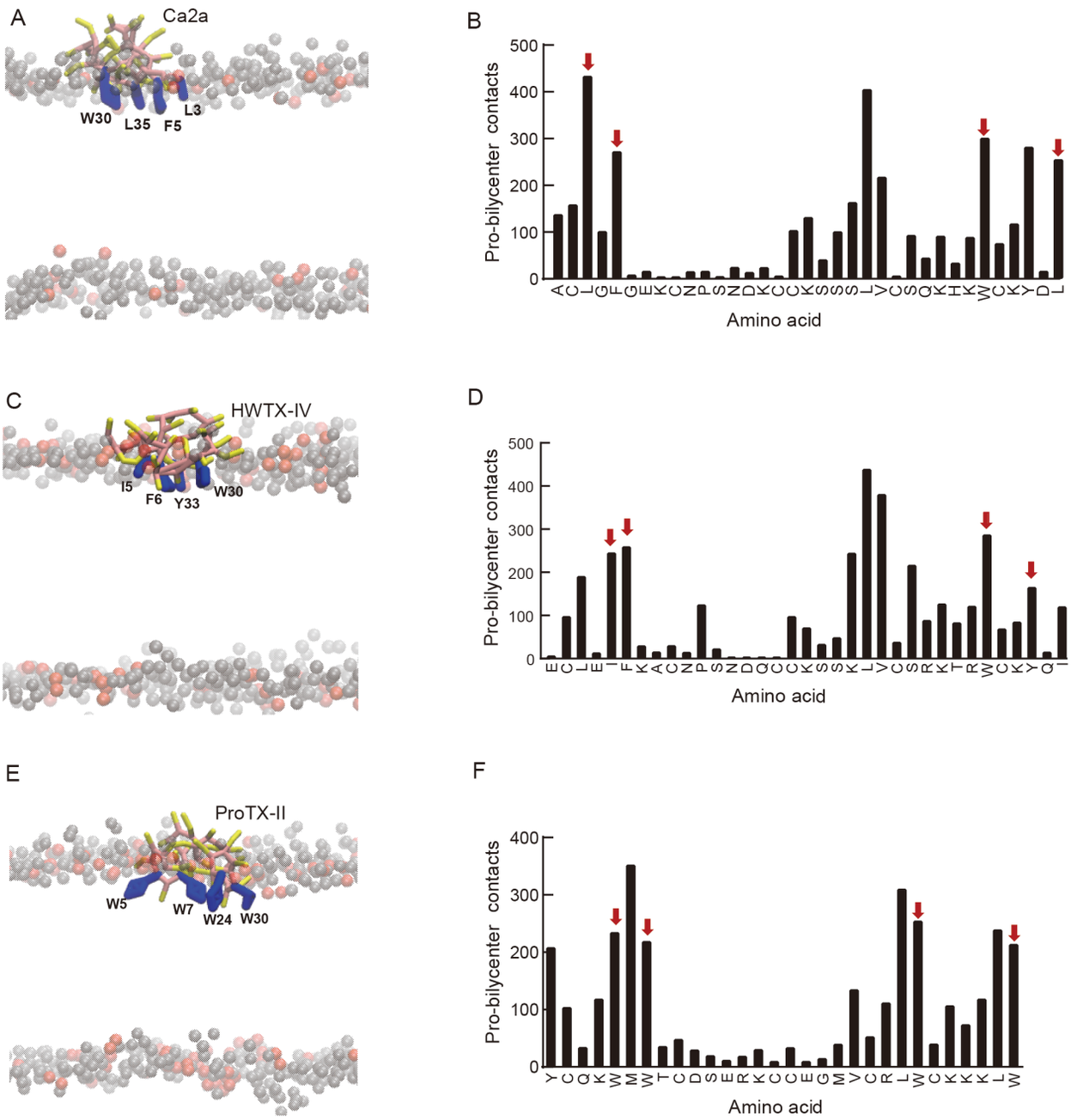

Figure 7 Quantitative analysis of toxin-membrane interactions and action models

A, C, E: Model diagram of Ca2a (A), HWTX-IV (C), and ProTX-II (E) with cell membrane, respectively. Residues inserted in cell membrane are labeled. Only lipid headgroups are presented, and POPC and POPS are in red and gray, respectively. B, D, F: Plots of pro-bilycenter contact scores for residues in Ca2a (B), HWTX-IV (D), and ProTX-II (F) interacting with cell membrane, respectively. Residues inserted into cell membrane in Figures A, C, and E are labeled as red arrows.

interactions are important for peptides to target their receptors. Here, we analyzed the interactions of several NaSpTx Family I toxins with cell membranes using molecular simulation. Three toxins showed similar properties when interacting with cell membranes, including peptide-membrane action intensity, distance, and insertion depth (Figure 6), although residue activities differed slightly (Figure 7). These findings provide evidence that NaSpTx Family I toxins share similar structures, underlying their activity on Nav1.7 channel.

As NaSpTx Family I toxins interact with the cell membrane, we performed peptide mutations and found that Ca2a mutations resulted in a loss of activity toward the Nav1.7 channel (Figure 4), including the F5, W30, and Y33 residues, which are required for toxin insertion into the cell membrane. These results confirmed that interactions of toxins with the cell membrane enhance their activity against ion channels.

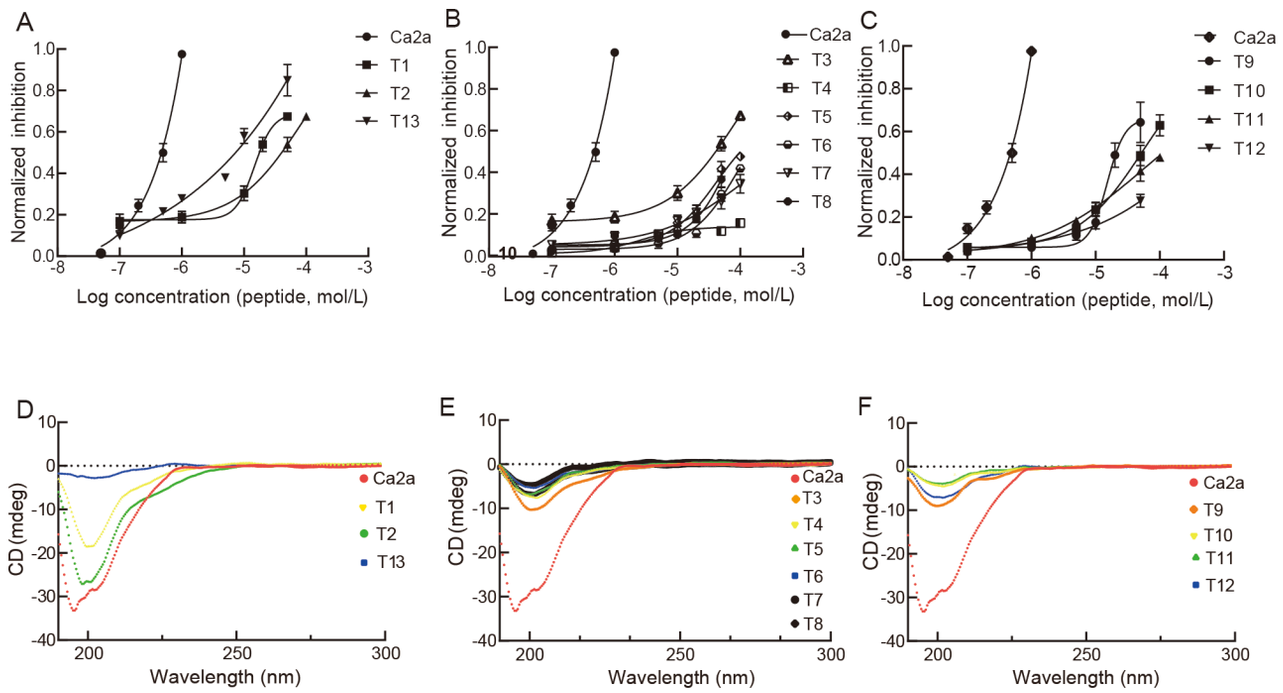

Figure 8 Effects of truncated peptides from Ca2a on hNav1.7

A–C: Dose curves of truncated peptides from Ca2a on hNav1.7. Peptides were sorted into three groups (A, B, and C) based on inhibitory activity. D–F: CD spectra showing that truncated peptides retained skeletal structure, corresponding to A–C.

Table 1 Sequences of truncated peptides and inhibition of hNav1.7

Peptide	Sequence	hNav1.7 IC_{50} (μmol/L)
Ca2a	ACLGFGEKCNPSNDKCCKSSSLVCSQKHKWCKYDL	0.487
T1	CLGFGEKC------CCKSSSLVCSQKHKWCKY	14.71
T2	CLGFGEKCNPS--KCCK--SLVC-QKHKWCKY	16.49
T3	CLGFGEKCN--NDKCCK--SLVC-QKHKWCKY	39.59
T4	CLGFGEKCN---DKCCKSSS--CSQKHKWCKY	>100
T5	CLGFGEKCN---DKCCKSSSL-CSQKHKWCKY	>100
T6	CLGFGEKCN---DKCCKSSS-VCSQKHKWCKY	>100
T7	CLGFGEKCNPS-DKCCKSSS-VCSQKHKWCKY	>100
T8	CLGFGEKC-PSNDKCC-SSSLVCSQKHKWCKY	>100
T9	CLGFGEKCNPSND-CCKSSSLVCSQKHKWCKY	67.31
T10	CLGFGEKCNPSN-KCCKSSSLVCSQKHKWCKY	53.55
T11	CLGFGEKCNPS-DKCCKSSSLVCSQKHKWCKY	49.18
T12	CLGFGEKCNP--D-CCK---LVCSQK--WCKY	>50
T13	CLGFGEKCN---DKCCK---LVCSQ-HKWCKY	8.89

Remarkably, cells were lost in patch-clamp recordings when certain Ca2a mutants were perfused at concentrations exceeding 30 μmol/L, possibly due to interactions of these peptides with the cell membrane. Insertion into the cell membrane has been reported for other toxins. Notably, tarantula toxins containing an inhibitor cystine knot in the backbone target most voltage-gated channels, stretch-activated cation channels, ligand-gated ion channels (Bosmans et al., 2006). Gating modifier toxins that modulate voltage-gated ion channels can interact with the cell membrane due to their amphipathic properties (Xu et al., 2019). For example, VsTx-I and PaTx-I can insert into POPE/POPG (3:1) and POPC/POPG (1:1) and HWTX-IV, Hd1a, HNTX-IV, and CcoTX-I can moderately bind to POPE/POPS (4:1).

Double-mutant cycle analysis is a powerful fool for the binding of toxins to ion channels and has been applied to facilitate the design of receptor-selective ligands (Horovitz, 1996). For instance, the binding sites of STX (Thomas-Tran & Du Bois, 2016) and μ-conotoxin (Chang et al., 1998) on skeletal muscle Na^+ channels were identified via double-mutant cycle analysis. Here, to further analyze the interactions of Ca2a with Nav1.7, we performed double-mutant cycle analysis. Results indicated that the K32A mutant of Ca2a had

similar inhibitory activity against the E818A mutant and WT of Nav1.7, and the E818A mutation of Nav1.7 decreased the binding of the K32A mutant and WT of Ca2a (Figure 4B, C, E). These results suggest that disruption of residue K32 in Ca2a or residue E818 in Nav1.7 (or both) may equally reduce the binding of Ca2a to Nav1.7. In contrast, the K27A mutant of Ca2a lost its affinity to E818 of Nav1.7, suggesting that residue K27 in Ca2a may not interact with residue 818 of Nav1.7, with a different site in Nav1.7 potentially binding to Ca2a.

We also explored the role of loop 2 in Ca2a regarding inhibitory activity against Nav1.7. The NaSpTx Family I toxins exhibited diversity in loop 2 sequences (Figure 1) and deletion of loop 2 in Ca2a resulted in a significant reduction in affinity to Nav1.7 (Figure 8A, C). The deletion of two residues (L22 and V23) in loop 3 in Ca2a resulted in markedly lower inhibitory activity against the channel (Figure 8C), which may be due to changes in the orientation of residues in Ca2a. Surprisingly, mutation of alanine and deletion of K18 in Ca2a resulted in a significant change in its affinity to Nav1.7 (Figures 4C, 8C), thus providing hints for peptide design. Furthermore, the shorter peptide T13 retained its function on the channel. The skeletons of all peptides were almost unchanged (Figure 8D–F). These findings indicate that residues in loop 2 are critical for the binding of Ca2a to Nav1.7, although deletion of loop 2 in Ca2a does not affect skeletal structure.

In summary, we studied and compared the structural and functional universality of NaSpTx Family I toxins, including Ca2a. Firstly, based on sequence alignment and homology modeling, the NaSpTx Family I toxins showed highly conserved structures. Secondly, molecular docking analysis indicated that the NaSpTx Family I toxins bonded to the domain II S3–S4 linker in Nav1.7, and E818 in Nav1.7, as a critical residue for peptide bonding, was identified in most NaSpTx Family I toxins, including Ca2a. Lastly, Ca2a and other toxins showed similar features when interacting with the cell membrane and several hydrophobic residues played critical roles in the insertion of Ca2a into the cell membrane. Importantly, based on double-mutant cycle analysis, K32 in Ca2a directly interacted with E818 in Nav1.7 and mutation of residues in loop 4 reduced channel affinity. Deletion of loop 2 residues in Ca2a dramatically reduced activity against Nav1.7 but did not affect the Ca2a skeleton. Thus, NaSpTx Family I toxins shared several structural and functional characteristics.

DATA AVAILABILITY

All data in the manuscript were submitted to the Science Data Bank database (DOI: 10.24272/j.issn.2095-8137.2022.185).

COMPETING INTERESTS

The authors declare that they have no competing interests.

AUTHORS' CONTRIBUTIONS

F.C.Y. performed most electrophysiological and molecular docking experiments. F.D.S. and H.L.A. completed dynamics simulation analyses. L.Z. and B.H. performed peptide synthesis. M.Q.R, C.W.D., and F.C.Y. designed the experiments, analyzed the data, and wrote the manuscript. All authors read and approved the final version of the manuscript.

REFERENCES

Agwa AJ, Lawrence N, Deplazes E, Cheneval O, Chen RM, Craik DJ, et al. 2017. Spider peptide toxin HwTx-IV engineered to bind to lipid membranes has an increased inhibitory potency at human voltage-gated sodium channel hNaV1.7. *Biochimica et Biophysica Acta* (*BBA*) - *Biomembranes*, **1859**(5): 835–844.

Ahuja S, Mukund S, Deng LB, Khakh K, Chang E, Ho H, et al. 2015. Structural basis of Nav1.7 inhibition by an isoform-selective small-molecule antagonist. *Science*, **350**(6267): aac5464.

Bosmans F, Rash L, Zhu SY, Diochot S, Lazdunski M, Escoubas P, et al. 2006. Four novel tarantula toxins as selective modulators of voltage-gated sodium channel subtypes. *Molecular Pharmacology*, **69**(2): 419−429.

Cardoso FC, Lewis RJ. 2019. Structure-function and therapeutic potential of spider venom-derived cysteine knot peptides targeting sodium channels. *Frontiers in Pharmacology*, **10**: 366.

Carstens BB, Clark RJ, Daly NL, Harvey PJ, Kaas Q, Craik DJ. 2011. Engineering of conotoxins for the treatment of pain. *Current Pharmaceutical Design*, **17**(38): 4242−4253.

Chang NS, French RJ, Lipkind GM, Fozzard HA, Dudley S. 1998. Predominant interactions between μ-conotoxin Arg-13 and the skeletal muscle Na^+ channel localized by mutant cycle analysis. *Biochemistry*, **37**(13): 4407−4419.

Cox JJ, Reimann F, Nicholas AK, Thornton G, Roberts E, Springell K, et al. 2006. An *SCN9A* channelopathy causes congenital inability to experience pain. *Nature*, **444**(7121): 894−898.

Cummins TR, Dib-Hajj SD, Waxman SG. 2004. Electrophysiological properties of mutant $Na_v1.7$ sodium channels in a painful inherited neuropathy. *Journal of Neuroscience*, **24**(38): 8232−8236.

de Lera Ruiz M, Kraus RL. 2015. Voltage-gated sodium channels: structure, function, pharmacology, and clinical indications. *Journal of Medicinal Chemistry*, **58**(18): 7093−7118.

Dib-Hajj SD, Yang Y, Black JA, Waxman SG. 2013. The $Na_V1.7$ sodium channel: from molecule to man. *Nature Reviews Neuroscience*, **14**(1): 49−62.

Du CW, Li JM, Shao ZC, Mwangi J, Xu RJ, Tian HW, et al. 2019. Centipede KCNQ inhibitor SsTx also targets $K_V1.3$. *Toxins* (*Basel*), **11**(2): 76.

Faber CG, Hoeijmakers JGJ, Ahn HS, Cheng XY, Han CY, Choi JS, et al. 2012. Gain of function $Na_V1.7$ mutations in idiopathic small fiber neuropathy. *Annals of Neurology*, **71**(1): 26−39.

Hayes F, Van Melderen L. 2011. Toxins-antitoxins: diversity, evolution and function. *Critical Reviews in Biochemistry and Molecular Biology*, **46**(5): 386−408.

Horovitz A. 1996. Double-mutant cycles: a powerful tool for analyzing protein structure and function. *Folding and Design*, **1**(6): R121−R126.

Kalia J, Milescu M, Salvatierra J, Wagner J, Klint JK, King GF, et al. 2015. From foe to friend: using animal toxins to investigate ion channel function. *Journal of Molecular Biology*, **427**(1): 158−175.

Kalman K, Pennington MW, Lanigan MD, Nguyen A, Rauer H, Mahnir V, et al. 1998. ShK-Dap^{22}, a potent Kv1.3-specific immunosuppressive polypeptide. *Journal of Biological Chemistry*, **273**(49): 32697−32707.

Klint JK, Senff S, Rupasinghe DB, Er SY, Herzig V, Nicholson GM, et al. 2012. Spider-venom peptides that target voltage-gated sodium channels:

pharmacological tools and potential therapeutic leads. *Toxicon*, **60**(4): 478−491.

Klint JK, Smith JJ, Vetter I, Rupasinghe DB, Er SY, Senff S, et al. 2015. Seven novel modulators of the analgesic target $Na_V1.7$ uncovered using a high-throughput venom-based discovery approach. *British Journal of Pharmacology*, **172**(10): 2445−2458.

Lawrence N, Wu B, Ligutti J, Cheneval O, Agwa AJ, Benfield AH, et al. 2019. Peptide-membrane interactions affect the inhibitory potency and selectivity of spider toxins ProTx-II and GpTx-1. *ACS Chemical Biology*, **14**(1): 118−130.

Li DL, Xiao YC, Xu X, Xiong X, Lu SY, Liu ZH, et al. 2004. Structure-activity relationships of hainantoxin-IV and structure determination of active and inactive sodium channel blockers. *Journal of Biological Chemistry*, **279**(36): 37734−37740.

Liu ZH, Cai TF, Zhu Q, Deng MC, Li JY, Zhou X, et al. 2013. Structure and function of hainantoxin-III, a selective antagonist of neuronal tetrodotoxin-sensitive voltage-gated sodium channels isolated from the Chinese bird spider *Ornithoctonus hainana*. *Journal of Biological Chemistry*, **288**(28): 20392–20403.

Luo L, Li BW, Wang S, Wu FM, Wang XC, Liang P, et al. 2018. Centipedes subdue giant prey by blocking KCNQ channels. *Proceedings of the National Academy of Sciences of the United States of America*, **115**(7): 1646−1651.

Marrink SJ, Risselada HJ, Yefimov S, Tieleman DP, de Vries AH. 2007. The MARTINI force field: coarse grained model for biomolecular simulations. *The Journal of Physical Chemistry B*, **111**(27): 7812−7824.

McCormack K, Santos S, Chapman ML, Krafte DS, Marron BE, West CW, et al. 2013. Voltage sensor interaction site for selective small molecule inhibitors of voltage-gated sodium channels. *Proceedings of the National Academy of Sciences of the United States of America*, **110**(29): E2724−2732.

Minassian NA, Gibbs A, Shih AY, Liu Y, Neff RA, Sutton SW, et al. 2013. Analysis of the structural and molecular basis of voltage-sensitive sodium channel inhibition by the spider toxin huwentoxin-IV (μ-TRTX-Hh2a). *Journal of Biological Chemistry*, **288**(31): 22707−22720.

Minett MS, Nassar MA, Clark AK, Passmore G, Dickenson AH, Wang F, et al. 2012. Distinct Nav1.7-dependent pain sensations require different sets of sensory and sympathetic neurons. *Nature Communications*, **3**: 791.

Payandeh J, Gamal El-Din TM, Scheuer T, Zheng N, Catterall WA. 2012. Crystal structure of a voltage-gated sodium channel in two potentially inactivated states. *Nature*, **486**(7401): 135−139.

Payandeh J, Scheuer T, Zheng N, Catterall WA. 2011. The crystal structure of a voltage-gated sodium channel. *Nature*, **475**(7356): 353−358.

Schmalhofer WA, Calhoun J, Burrows R, Bailey T, Kohler MG, Weinglass AB, et al. 2008. ProTx-II, a selective inhibitor of $Na_V1.7$ sodium channels, blocks action potential propagation in nociceptors. *Molecular Pharmacology*, **74**(5): 1476−1484.

Shcherbatko A, Rossi A, Foletti D, Zhu GY, Bogin O, Casas MG, et al. 2016. Engineering highly potent and selective microproteins against Nav1.7 sodium channel for treatment of pain. *Journal of Biological Chemistry*, **291**(27): 13974−13986.

Shen HZ, Liu DL, Wu K, Lei JL, Yan N. 2019. Structures of human $Na_v1.7$ channel in complex with auxiliary subunits and animal toxins. *Science*, **363**(6433): 1303−1308.

Sun FD, Ding XF, Xu LD, Liang JF, Chen L, Luo SZ. 2017. A molecular dynamics study of the short-helical-cytolytic peptide assembling and bioactive on membrane interface. *The Journal of Physical Chemistry C*, **121**(32): 17263−17275.

Sun FD, Schroer CFE, Palacios CR, Xu LD, Luo SZ, Marrink SJ. 2020. Molecular mechanism for bidirectional regulation of CD44 for lipid raft affiliation by palmitoylations and PIP2. *PLoS Computational Biology*, **16**(4): e1007777.

Tang DF, Xu JH, Li YP, Zhao P, Kong XJ, Hu HL, et al. 2021. Molecular mechanisms of centipede toxin SsTx-4 inhibition of inwardly rectifying potassium channels. *Journal of Biological Chemistry*, **297**(3): 101076.

Thomas-Tran R, Du Bois J. 2016. Mutant cycle analysis with modified saxitoxins reveals specific interactions critical to attaining high-affinity inhibition of $hNa_V1.7$. *Proceedings of the National Academy of Sciences of the United States of America*, **113**(21): 5856−5861.

Weiss J, Pyrski M, Jacobi E, Bufe B, Willnecker V, Schick B, et al. 2011. Loss-of-function mutations in sodium channel $Na_v1.7$ cause anosmia. *Nature*, **472**(7342): 186−190.

Wisedchaisri G, Tonggu L, El-Din TMG, McCord E, Zheng N, Catterall WA. 2021. Structural basis for high-affinity trapping of the $Na_V1.7$ channel in its resting state by tarantula toxin. *Molecular Cell*, **81**(1): 38−48.e4.

Xiao YC, Bingham JP, Zhu WG, Moczydlowski E, Liang SP, Cummins TR. 2008. Tarantula huwentoxin-IV inhibits neuronal sodium channels by binding to receptor site 4 and trapping the domain ii voltage sensor in the closed configuration. *Journal of Biological Chemistry*, **283**(40): 27300−27313.

Xiao YC, Blumenthal K, Jackson II JO, Liang SP, Cummins TR. 2010. The tarantula toxins ProTx-II and huwentoxin-IV differentially interact with human $Na_v1.7$ voltage sensors to inhibit channel activation and inactivation. *Molecular Pharmacology*, **78**(6): 1124−1134.

Xu H, Li TB, Rohou A, Arthur CP, Tzakoniati F, Wong E, et al. 2019. Structural basis of Nav1.7 inhibition by a gating-modifier spider toxin. *Cell*, **176**(4): 702−715.e14.

Yang SL, Xiao Y, Kang D, Liu J, Li Y, Undheim EAB, et al. 2013. Discovery of a selective $Na_V1.7$ inhibitor from centipede venom with analgesic efficacy exceeding morphine in rodent pain models. *Proceedings of the National Academy of Sciences of the United States of America*, **110**(43): 17534−17539.

Yu FH, Catterall WA. 2003. Overview of the voltage-gated sodium channel family. *Genome Biology*, **4**(3): 207.

Zhang Y. 2015. Why do we study animal toxins?. *Zoological Researc*h, **36**(4): 183–222.

Zhang YX, Peng DZ, Huang B, Yang QC, Zhang QF, Chen MZ, et al. 2018. Discovery of a novel $Na_v1.7$ inhibitor from *Cyriopagopus albostriatus* venom with potent analgesic efficacy. *Frontiers in Pharmacology*, **9**: 1158.

Zhang YX, Wang L, Peng DZ, Zhang QF, Yang QC, Li JY, et al. 2021. Engineering of highly potent and selective HNTX-III mutant against $hNa_v1.7$ sodium channel for treatment of pain. *Journal of Biological Chemistry*, **296**: 100326.